Modeled Oceanic Response and Sea Surface Cooling to Typhoon Kai-Tak

Yu-Heng Tseng[1], Sen Jan[2], David E. Dietrich[3], I-I Lin[1], Ya-ting Chang[4], T. Y. Tang[4]

[1]Department of Atmospheric Sciences, National Taiwan University

1, Sec. 4, Roosevelt Rd., Taipei 10617, Taiwan, R.O.C.

[2]Institute of Hydrological and Oceanic Sciences, National Central University

300 Jung-da Rd., Jung-li 32001, Taiwan, R.O.C.

[3]AcuSea Inc.,

8450-101 Via Sonoma, La Jolla, CA92037, USA

[4]Institute of Oceanography, National Taiwan University

1, Sec. 4, Roosevelt Rd., Taipei 10617, Taiwan, R.O.C.

Abstract

The ocean response to typhoon Kai-Tak is simulated using a fourth-order accurate, basin-scale ocean model. The surface winds of typhoon Kai-Tak were obtained from QuikSCAT satellite images blended with the ECMWF wind fields. An intense nonlinear mesoscale eddy is generated in the northeast South China Sea (SCS) with a Rossby number of O(1) and on a 50–100km horizontal scale. Inertial oscillation is clearly observed. Advection dominates as the strong wind shear drives the mixed layer flows outward, away from the typhoon center, thus forcing upwelling from deep levels with a high upwelling velocity (>30 m/day). A drop in sea surface temperature (SST) of more than 9°C is found in both observation and simulation. We attribute this significant SST drop to the influence of the slow moving typhoon, initial stratification and bathymetry-induced upwelling in the northeast of the SCS where the typhoon hovered.

1. Introduction

It is well known that tropical cyclones (TCs), also known as typhoons (in the Pacific) and hurricanes (in the Atlantic), draw their energy from warm ocean (Emanuel et al., 1986). Through air-sea interaction, ocean supplies energy for typhoon's intensification (Emanuel et al., 1986; Moon et al., 2007, 2008; Lin et al., 2009a). Pre-existing ocean mesoscale features and subsurface structures may be far more important than SST alone in the heat and moisture fluxes feeding the storm. Shay et al. (2000) noted an abrupt change in the intensity of hurricane Opal (9/28-10/5, 1995) when it passed over a large warm core eddy (WCE). Hurricane Katrina in August 2005 also showed a very similar intensification while passing over the Loop Current and WCE regions. Lin et al. (2005;2008) noted the critical role of warm ocean eddies in the western North Pacific category-5 typhoons in observing that 30% of these supertyphoons are fuelled by the warm ocean features. Wu et al. (2007) used simple coupled typhoon-ocean model to study the role of warm and cold eddies in typhoon's intensification. Typhoons also cause significant SST cooling which provides negative feedback to the overlying storm by weakening its intensity. For example, satellite images showed that SST dropped more than 9°C and 11°C in response to the passage of typhoons Kai-Tak (Lin et al., 2003) and Ling-Ling (Shang et al., 2008), respectively. Wu et al. (2008) studied the air–sea interaction between typhoon Nari and the Kuroshio current using satellite observations and an ocean model. The intensity of typhoon Nari varied a few times when it crossed over the Kuroshio. These examples demonstrated the role of warm (cold) oceanic features in providing a positive (negative) feedback to the overlying storms by causing intensification (weakening) of the storms.

In general, the primary mechanisms accounting for the sea surface cooling caused by TCs include mixed layer depth (vertical mixing/entrainment) and thermocline depth, exchange of air–sea heat fluxes, and the storm's intensity and translation speed (Price, 1981; Lin et al., 2009b). Intense, slow moving typhoons usually cause a larger SST response. Since evaporation due to high winds over warm water sustains the thermodynamic cycle of a TC, SST cooling is thought to inhibit cyclone intensification, preventing the cyclones from attaining their potential intensity (Emanuel, 1999, 2001). When a typhoon encounters warm ocean features, SST cooling may be greatly suppressed primarily due to deep mixed-layer and thermocline depths (Wu et al., 2008).

Early studies of upper-ocean response to TCs include field observations (e.g. Shay et al., 1989; Jacob et al., 2000) and three-dimensional numerical ocean models (Price, 1981; Price et al., 1994). Recent studies emphasized the understanding of the dynamic processes and interactions with the atmosphere, ocean heat content and ocean currents (e.g. Wu et al., 2008; Tsai et al., 2008; Oey et al., 2007; Sheng et al., 2007). Typically, the ocean's response to TCs can be divided into two stages: forced and relaxation stages. During the forced stage, the hurricane winds drive the mixed layer currents, causing SST cooling by vertical mixing (entrainment) and air–sea heat exchange (e.g. loss of latent heat flux). The barotropic response consists of a non-geostrophic component which changes the sea surface height (a part of the inertia gravity response). The relaxation stage response follows a hurricane's passage, and is primarily influenced by inertial gravity oscillations excited by the TC. The mixed-layer velocity oscillates with a near-inertial period, and hence so too do the divergence and the associated upwelling and downwelling (Tsai et al., 2008).

However, no study has focused on the causes and mechanisms of the significant

78 temperature drops for particular TCs. Oceanic responses to TCs differ from one to
79 another in several respects, and thereby make the processes difficult to study. This is
80 further complicated by pre-existing oceanic features that modulate the upper ocean
81 heat, mass and momentum balance due to advection. These mesoscale features need
82 to be resolved in order to study the oceanic response. The extremely large amount of
83 surface cooling in typhoon Kai-Tak was found mainly because of the continuous wind
84 forced upwelling, a relatively shallow and warm mixed layer in the SCS and the local
85 bathymetry of the SCS. The upwelling was enhanced by the typhoon's
86 quasi-stationary motion. Similarly, a shallow mixed layer depth (~30 m) was also
87 observed in the case of typhoon Ling-Ling and may have contributed to the 11°C
88 temperature drop after its passage (Shang et al., 2008). The coastal upwelling and
89 pre-existing ocean features significantly enhanced pronounced sea surface cooling.

90 The main objectives of this paper are (1) to study the effect of a slow moving typhoon
91 (Kai-Tak) in the South China Sea; (2) to quantify the physical processes which control
92 the upper ocean thermal structure and strong surface cooling during the typhoon's
93 passage; and (3) to assess the model's ability to reproduce the observed behavior of
94 the oceanic responses to a typhoon without data assimilation. This paper is organized
95 as follows: Section 2 describes the passage of typhoon Kai-Tak and relevant
96 observations. Section 3 details the model configuration, initial and boundary
97 conditions and model experiments. Section 4 compares the simulated results with
98 observations followed by a qualitative description of the oceanic response to typhoon
99 Kai-Tak. The mechanism that causes the significant SST drop is also investigated. The
100 summary and conclusion are given in Section 5.

101

2. Typhoon Kai-Tak and Observations

Typhoon Kai-Tak was declared a category 2 TC on the Saffir-Simpson hurricane scale. It lingered with slow speeds (0-1.4 m/s) in the northern SCS from July 5-8, 2000 before moving rapidly northwards thereafter (see Figure 1 for the storm track). The typhoon remained almost at rest during July 6-8. Remote sensed data provides an opportunity to investigate the surface behavior. Two remote sensed datasets were used in an earlier study (Lin et al., 2003); QuikSCAT and the Tropical Rainfall Measuring Mission (TRMM) Microwave Imager (TMI), respectively. The ocean surface wind vector (QuikSCAT) and the sea surface temperature (TMI) were measured day and night under both clear and cloudy conditions. The cloud penetrating capability of TMI allows the entire area of entrainment (location of a phytoplankton bloom patch) to be sensed. Here we have also incorporated QuikSCAT to provide an adequate wind forcing information in the model simulation. Figure 2 shows the daily averaged wind fields taken from QuikSCAT, illustrating how the typhoon lingered for several days in the northeast SCS during its passage of the SCS. More details about the wind forcing are provided in the next section.

Before typhoon Kai-Tak's arrival, the SCS was characterized by predominantly warm SST greater than 30°C (Lin et al., 2003). Based on an average of ten-day TOPEX/Poseidon (T/P) satellite images, the Sea Surface Height Anomaly (SSHA) showed relatively calm eddy fields in the northeast SCS prior to July 5 (Figure 1(a)). The typhoon's strong winds (20-40 m/s) dominated the QuikSCAT wind field during July 7 to July 8 (Figure 2). Immediately after typhoon Kai-Tak's departure, a cold SST pool, with temperatures of 21.5-24°C (118-120°E, 19-20.5°N) of a size comparable to Kai-Tak's 150 km RMW (Radius of Maximum Wind), was observed and co-located with the typhoon's track. The minimum SST of 21.5°C was found at the center

(118.9°E, 19.9°N) of the cold pool (Lin et al., 2003). In comparison with the pre-typhoon conditions, the SST had dropped by as much as 8-9°C. This cold pool slowly decayed after the passage of the typhoon, but still maintained a low temperature of 25°C. After the passage of typhoon Kai-Tak, the formation of a cyclonic eddy was observed, which is clearly intensified in the T/P image in Figure 1(b). The location, scale and peak of the growing cyclonic eddy (Figure 1(b)) matched well with the cold SST pool shown in Lin et al. (2003). The cyclonic eddy lasted for more than two weeks (Figure 1(b)). From these satellite images, the westward propagating Rossby waves and eddy fields in the North Pacific Ocean were identified while the cyclonic eddy grew in the northeast SCS.

Some in-situ hydrographic surveys were conducted in the northeast SCS during the year 2000, including the South East Asia Time-series (SEATS) station (116°E, 18°N) in July 2000 and the Kuroshio Upstream Dynamics Experiment (KUDEX) mooring station KA1, labeled as red circular spot "○" in Figure 2 (see Table 1 for detailed information). Both stations were under the influence of typhoon Kai-Tak. Some comparison with station KA1 will be discussed in Section 4. The initial stratification taken from the SEATS station (red diamond, "◇") is shown in Figure 2. The surface mixed layer, with a temperature of 29°C, was only about 20-30 m deep (Figure 2 bottom right). After the passage of typhoon Kai-Tak, the minimum temperature in the cold pool dropped to 21.6°C, which corresponded to the initial temperature at 71 m depth. The other station used in the comparison is an observation station at the southern tip of Taiwan (ST, labeled as a red square "□" in Figure 2).

Table 1: KUDEX station KA1

Station	Location	Sampling interval	Local depth	Data type	Depth (m)
KA1	118°06'E, 20°23'N	60 min	2885 m	ADCP	30-210-10
				T	230

3. Numerical Simulations

3.1 Model setup and description

The Dual grid Pacific Ocean Model (DUPOM) used herein is based on the fourth-order accurate, collocated Arakawa-A grid DieCAST (Dietrich/Center for Air Sea Technology) model (Dietrich, 1997; Dietrich et al, 2004a; Tseng et al., 2005; Tseng and Breaker, 2007). The control volume equations include fluxes of the conservation properties (momentum, heat and salt) across control volume faces. The model domain covers the entire North Pacific Ocean, ranging from 30°S to 60°N and from 100°E to 80°W. To reduce the computational time, a dual grid approach was adopted based on a multiple grid framework, which uses higher resolutions to resolve eddies more realistically (Dietrich et al., 2008; Dietrich et al., 2004a). A 1/8° resolution was used west of 150°E, where a finer resolution was required to resolve the detailed Kuroshio Current and regional circulations, and a 1/4° resolution was used east of 150°E (Figure 3). The grids are fully two-way coupled at each coarser time step (time steps differ for the two grids) with a single coarse grid overlapping (i.e. 2×2 in fine grid cells). The meander and eddy exchanges are seamless at the interface without inter-grid sponge layers or special treatments. Further details about the multiple grid approach can be found in Dietrich et al. (2008). Model bathymetry was interpolated from unfiltered ETOPO2 depth data, supplemented with the Taiwan National Center for Ocean Research 1 minute depth archive for the Asian seas. The vertical resolution is linear-exponentially stretched by 26 layers, with a 6-m thick top layer. Both grids share the same vertical grid. Within each grid, longitudinal resolution is uniform and latitudinal resolution is generated in such a manner that varying

174 latitude and longitude grid increments are equal everywhere (Mercator grid).

175 The surface wind forcing in the basic model is obtained from the interpolated monthly
176 Hellerman and Rosenstein winds (Hellerman and Rosenstein, 1983). The Levitus'94
177 climatology (Levitus and Boyer, 1994) is used to initialize the model and to determine
178 its surface sources of heat and fresh water (E-P) using the non-damping approach
179 described in Dietrich et al. (2004b). The northern boundary is closed and the southern
180 boundary condition (30°S) is slowly nudging toward climatology in a sponge layer.
181 The bottom is insulated, with non slip conditions parameterized by a nonlinear bottom
182 drag.

183 Simulation of mixed layer deepening and cooling during the typhoon's passage
184 strongly depends on the choice of vertical mixing scheme. Except for vertical mixing
185 parameters, the present model is very similar to the DieCAST model adaptation used
186 to simulate the response to Hurricane Katrina (Dietrich, et al., 2007). Recent studies
187 of upper ocean response to hurricanes, based on several bulk mixed layer entrainment
188 schemes, have revealed significant differences in the heat and mass budgets (Jacob et
189 al., 2000; Jacob and Shay, 2003; Prasad and Hogan, 2007). The suitability of any
190 particular scheme is still subject to debate. Except for sub-grid scale vertical mixing
191 parameters, the present model is very similar to that used by Sheng et al. (2006) and
192 by Dietrich et al (2008). The model's sub-grid scale vertical mixing is parameterized
193 by eddy diffusivity (for temperature and salinity) and viscosity (for momentum) using
194 a modified Price (1981) scheme as described in Sheng et al. (2006). This new scheme,
195 replacing the default Pacanowski and Philander (1982) scheme, was chosen to obtain
196 a better mixed layer due to the strong wind forcing during the passage of the typhoon.
197 Background lateral viscosity and diffusivity are 100 m^2/s and 200 m^2/s, respectively.

198

199 *3.2 Initial and boundary conditions*

200 This study emphasizes dynamic processes rather than the model's capability of
201 nowcasting or forecasting. The model approached a quasi-equilibrium status after a
202 few years of spinning up. The circulation pattern on July 1 of model year 23 was then
203 chosen as the initial condition for the simulation of typhoon Kai-Tak. Initial
204 temperature and salinity fields are based on the SEATS observations before typhoon
205 Kai-Tak's passage in July 2000. All model integrations were started on July 3 2000
206 (see Figure 1 for the typhoon's track).

207 The model was then driven by fields of 10 m wind stress extracted from six-hourly
208 2.5° ERA40. It is a well known fact that the ERA-40 product does not adequately
209 resolve TCs. In this study, we further blended the ERA-40 winds with the QuikSCAT
210 analyzed winds (Figure 2). Since the QuikSCAT data (twice per day) provided a more
211 realistic and high quality wind field and may not be consistent with the ERA-40, a
212 smoothing procedure was performed. We took the difference between the QuikSCAT
213 and ERA-40 winds at each of the discrete observations and times. This difference was
214 merged into an "extended winds window" (EWW) grid, which was larger than the
215 localized QuikSCAT wind field. The difference was then set to zero at the boundary of
216 EWW, followed by a Poisson spreader to spread the difference between the
217 QuikSCAT wind and the EWW grid boundaries. In order to minimize the nudging at
218 the EWW grid boundaries, the EWW should extend laterally at least an eddy size
219 beyond the QuikSCAT wind fields. Finally, the blended wind fields were then
220 interpolated back to the model domain for application.

221 Following Oey et al. (2006), the wind stress was calculated from the wind fields using

222 a bulk formula:

223 $C_d = 0.0012, \quad |u_a| \le 11$ m/s

224 $= 0.00049 + 0.000065\,|u_a|, \quad 11 < |u_a| \le 19$ m/s

225 $= 0.001364 + 2.34 \times 10^{-5}|u_a| - 2.3\times10^{-7}\,|u_a|^2, \quad 19 < |u_a| < 100$ m/s

226 where $|u_a|$ is wind speed (the maximum wind speed reached ~40 m/s from the
227 QuikSCAT). This formula modifies Large and Pond (1981) to incorporate the limited
228 drag coefficient for high wind speeds (Powell et al., 2003). All wind stresses were
229 assumed to be in dynes/cm^2 and of a magnitude less than 100 dynes/cm^2.

230

231 ## 4. Numerical Results

232 *4.1 Typhoon-induced circulation and inertial currents during typhoon Kai-Tak*

233 Figure 4 shows the equivalent sea surface height (SSH) superimposed by the surface
234 velocity vector for every 30 hours, after imposing the QuikSCAT wind forcing on July
235 3. The eyewall winds enhanced a strong, out-of-balance cyclonic flow, as indicated by
236 the vectors which revealed a large outward flow component of the cyclonically
237 spinning water. The wind-induced currents are frictionally driven by the wind, and
238 their pattern generally follows the wind field. After hour 90, the wind driven currents
239 were intensified and concentrated over the northeast SCS (July 6). The intense
240 nonlinear mesoscale vortex has a scale of ~100-150 km. The SSH fields showed that
241 typhoon Kai-Tak hovered over the SCS, and strengthened its cylonic circulation for a
242 few days. The slowly moving typhoon enhanced the cyclonic eddy to penetrate into

243 deeper layers (Wu et al., 2008).

244 During the passage of typhoons, a sudden change of the surface wind stress can
245 generate inertial motions in the upper ocean (Gill, 1982). In the north SCS, the
246 averaged inertial period was about 35 hr (~20°N). The TC-induced inertial motions
247 can last for two weeks or longer in some cases. We further compared the model
248 velocities with those measured at the ADCP mooring station KA1 (KUDEX). The
249 modeled zonal and meridional velocity (U and V, cm/s) components were compared
250 with the observed velocity profiles vertically at the same location (Figure 5). To
251 separate rapidly fluctuating inertial motions from other relatively low frequency
252 inertial currents, a six hour low-pass filter was applied to the observed currents.
253 Figure 5 shows the vertical profile comparison between the modeled and observed
254 velocity components. The sensitivity of turbulent parameterization is also evaluated in
255 the upper two panels. Both model and observation showed reasonably quasi-inertial
256 oscillations ~34 hr. The model using the modified Price scheme showed more
257 ordinary patterns, while the KA1 observation presented a larger variability. Using
258 QuikSCAT wind vectors, entrainment-induced mixed layer deepening was estimated
259 at ~100 m by a modified mixed layer turbulence parameterization (Sheng et al., 2006),
260 and varied with time (Figure 5). This parameterization appears to perform relatively
261 well compared with the traditional Pacanowski and Philander (1982), denoted by
262 PP82 in the current simulation, due to the larger typhoon-induced vertical mixing and
263 entrainment. The modeled mixed layer was shallower using the PP82
264 parameterization, resulting from insufficient vertical mixing in the surface mixed layer.
265 More comparison between different turbulent parameterizations is discussed later.

266 Figure 6 shows additional time series velocity components in the upper layer at four
267 different locations. The relative locations with respect to the typhoon center are west,

east, north and south (top to bottom). Large inertial currents were concentrated around the typhoon. The flow velocities also changed directions during the passage of typhoon Kai-Tak. Unlike the wind-driven currents, the inertial amplitudes in a fast moving typhoon are usually much larger on the right of the typhoon path than on the left. This amplitude asymmetry is particularly striking when the wind vectors rotate at roughly the same rate as the inertial motion (Chang and Anthes 1978; Price 1981). It is found that the amplitude asymmetry is not so clear in Figure 6 due to the slow movement of typhoon Kai-Tak. It appears that the inertial currents were not destroyed by the quasi-stationary typhoon Kai-Tak. These inertial motions lasted for a long time after typhoon Kai-Tak had passed from the observation region (Chen, 2006).

4.2 Sensitivity of turbulence parameterization

The role of mixing and upwelling was also examined using the observational profiles at ST. ST is a station located at the southern tip of Taiwan (see Figure 2 for the location). Since typhoon-induced turbulent mixing is difficult to resolve in the ocean model and cannot be easily parameterized, we attempted to further explore the influence of different turbulence parameterizations. Zedler et al. (2002) used four one-dimensional mixed layer models, namely Price-Weller-Pinkel (PWP), K Profile Parameterization (KPP), Mellor-Yamada 2.5 (MY), and a modified version of MY2.5 (MY2), to investigate the upper ocean's response to Hurricane Felix (1995). Temperature evolution was found to be sensitive to the parameterization schemes chosen. They also found that the sea surface cooling predicted by KPP model was closer to the observations than any of the other models. This is partially due to a special treatment for gradient Richardson number shear instability mixing in response to resolved shear in the ocean interior (Zedler et al., 2002).

292 The results of our model experiments are presented in Figure 7(a). The impacts of
293 turbulent parameterization were assessed by comparing SSTs, which showed
294 significantly different behaviors after July 5 when strong wind forcing took place.
295 Both PP82 and the modified Price scheme were examined. Similar to the observation,
296 the modeled SST using the modified Price scheme indicated two periods of cooling.
297 The cooling during the storm was primarily due to the strong wind-driven turbulent
298 mixing resulting from vigorous wind stress. It should be noted here that the mixing
299 generated by typhoon-induced internal waves is still not well represented in any
300 turbulent parameterization. Further cooling was possibly due to advection, upwelling
301 and further mixing. Apparently, the second period of cooling was missing in the case
302 using the PP82. This difference was not surprising, based on the different mixed layer
303 depths. This implied that the simple Richardson number based PP82 scheme provided
304 insufficient instability mixing and was consistent with the weaker and shallower
305 inertial oscillation response shown in Figure 5.

306 Our results supported the importance of realistic parameterization of turbulence in
307 modeling ocean response to tropical cyclones. The temperature evolution is most
308 sensitive to the turbulent mixing parameterization. The greater wind stress, resulting
309 from typhoon Kai-Tak in particular, may have affected the surface mixed layer
310 responses including internal gravity waves, mixed layer deepening and energy
311 redistribution (Zedler et al., 2002). These features could be altered significantly due to
312 different mixing parameterization. Unfortunately, to the best of our knowledge, no
313 ideal turbulent mixing parameterization is currently available for all circumstances.
314 Recent studies also showed that numerical dissipation and diffusion may interact with
315 turbulence schemes unless higher order, non-dissipative numerical methods are used
316 (e.g. Tseng and Dietrich, 2006; Tseng, 2008).

4.3 What caused the significant temperature drop during the passage of typhoon Kai-Tak?

A cool wake is usually a pronounced feature of a moving typhoon, and is significantly biased to the right side of the typhoon track (looking in the direction of the typhoon motion). This rightward bias of cooling has been attributed to the asymmetric turning (in time) of wind stress that arises from the translation of a vertical wind pattern (Price, 1981). For a slowly moving (or quasi-stationary) tropical cyclone such as typhoon Kai-Tak, the rightward bias is less pronounced (Lin et al., 2003), but a cool pool is still evident. Two extreme surface cooling events after the passage of typhoons (including typhoon Kai-Tak) are known to have occurred (>9°C) in the SCS (Lin et al., 2003; Shang et al., 2008). How did such a drastic response happen? Why did these two events of extreme SST cooling occur in the SCS?

Figure 8(a) shows the modeled temperature profiles along latitude 20.5°N (top) and longitude 119°E (bottom) during July 3-8. The SST started to cool down from July 5-7. Consistent with the satellite observations, the overall cool pool temperature dropped to ~22°C after July 8. The cool pool remained there for a few days and no further significant temperature drop was observed following the passage of typhoon Kai-Tak. This suggests that the upwelled thermocline may have reached the ocean surface while the surface layer was well mixed (Figures 5-6). Entrainment mixing is, in general, the primary mechanism accounting for the SST response (Price, 1981). However, for a slow moving cyclone (translation speed <=4 m/s), such as typhoon Kai-Tak, strong upwelling occurs with entrainment as a result of the persistent secondary outward near-surface flows, which must occur as part of the geostrophic

adjustment during the wind-forced spin-up of an ocean surface cyclonic vortex (Ekman pumping). Thus, the cooling due to surface mixed layer thickening may be significantly enhanced (Price, 1981). Figure 8(b) shows the horizontal distribution of the modeled SST after hour 90. The horizontal advection is important in the mixed layer heat balance during and subsequent to the passage of tropical cyclones (Price, 1981; Jacob et al., 2000). This contribution is particularly significant in the eddy region. The maximum cooling (and upwelling) is found in a ring around the core of the typhoon, which appears to start in the northeast corner of the typhoon where a wind-forced upslope flow may be involved. This initial cooling center appears to have been forced by the inertial dynamics of a fast wind-driven current up the shelfslope in the northeastern SCS. The downslope return flow can also create strong eddies by releasing potential energy, thus providing some significant mixing.

The thermocline displacement due to the typhoon-induced upwelling can be evaluated using the model results. Figure 9 further shows the time series temperature profile in the upper layer (<300 m) at different locations along latitude 20.5°N. The temperature dropped to a depth of more than 150 m near the typhoon center (~119°E in Figure 8(c) after July 6. The surface mixed layer kept cooling down and reached the minima at around July 8. Since the thermocline was shallow (Figure 2) prior to the passage of typhoon Kai-Tak, the deep water appeared to be upwelled to the surface near the typhoon center. This upwelling was also associated with strong mixed layer thickening, due to enhanced mixing and entrainment. The surface mixed layer not only thickened significantly but also mixed efficiently due to strong turbulence. The thermocline became much thinner due to the upwelled thermocline in the deeper layer. This mixed layer thickening (or thermocline thinning) occurred everywhere near the strong wind stress except for the far field at 116.5°E (Figure 9(a)) as expected. Some

366 previous studies have emphasized entrainment/mixing as the dominant term in the
367 mixed layer heat budget (Jacob and Shay, 2003). Jacob et al. (2000) suggested that
368 entrainment/mixing at the base of the mixed layer generally accounts for a large
369 portion of the cooling (75%-90%) based on observations. Inertial oscillations were
370 also identified from Figure 9. Based on the model results, we estimated that the
371 thermocline upwelled from depths of 70-100 m within the areas of maximum SST
372 change.

373 What intensified the cooling at the center of the cold patch? The pre-conditioned
374 shallow surface mixed layer could have played an important role. Qu et al. (2007)
375 showed that the isothermal depth in the northern South China Sea can exceed 70 m in
376 winter and fall below 20 m in summer near the continental slope south of China,
377 based on the World Ocean Database 2001 (WOD01). Consistent with our observations
378 in Figure 2, the monthly mean isothermal depth was at around 30-35 m in July where
379 typhoon Kai-Tak hovered (Qu et al., 2007). The thermocline in that area is generally
380 shallower during spring and summer. In the other extreme surface cooling event
381 during the passage of typhoon Ling-Ling, the mean thermocline for the area of
382 extreme cooling was of around 25-35 m (Qu et al., 2007). Apparently, the
383 preconditioned shallow mixed layers contributed significantly to the extremely cool
384 pool in both cases since the cold water below the thermocline was totally upwelled to
385 the surface. In addition, the cooling area of typhoon Ling-Ling was also associated
386 with a locally pre-existing cyclonic gyre from the T/P derived geopotential anomaly,
387 which appeared to be a sub-basin scale seasonal circulation driven by the winter
388 monsoon (Shang et al., 2008). Maximum cooling was found at the gyre center where
389 the thermocline was much shallower than usual condition (~30 m compared to the
390 more typical 50-100 m in winter). The pre-conditioned shallow mixed layer favored

391 more vigorous cooling. With much cooler water nearer the surface, less energy is
392 needed to lift the deeper water to the surface, resulting in large and rapid surface
393 cooling. Note that typhoon Kai-Tak was declared to be a category 2 typhoon whereas
394 typhoon Ling-Ling was classified as category 4.

395 The strong upwelling during the passage of typhoon Kai-Tak should also be
396 associated with other upwelling mechanisms, so that waters below the thermocline
397 could be effectively upwelled to the surface. Figure 10 shows daily averaged vertical
398 subsidence calculated at 45 m depth on July 7 (day 5); it shows strong vertical
399 upwelling (negative subsidence is upward) near the cold pool when the typhoon
400 hovered in the northeastern SCS. The averaged maximum vertical velocity reached 30
401 m/day near the typhoon center, indicating a very large amount of vertical convection.
402 The thermocline slope in Figure 9(c) shows that the instantaneous vertical velocity
403 can be even larger. The continuous Ekman pumping during July 5-8 due to the
404 lingering tail of the typhoon is also enhanced by the topographical upwelling (Figure
405 11). Figure 11 shows the bottom currents flowing along the topography. The isobaths
406 are also plotted in Figure 11.Very strong alongshore currents occurred near the
407 Philippine coastal shelf. A quasi-cyclonic eddy associated with large upward motions
408 can be observed near the center of the cold pool. This near bottom cyclonic eddy was
409 collocated with the typhoon center, and was strengthened by the bottom bathymetry.
410 This deep eddy, resulting from the bathymetry steering, may have enhanced the strong
411 upwelling locally. Similar bathymetry or deep canyon enhanced upwelling can also be
412 found in Monterey Bay, USA (e.g. Tseng et al., 2005; Tseng and Breaker, 2007). This
413 enhancement is usually associated with strong cyclonic eddy.

414 These features are also consistent with other earlier observations. In Hurricane Ivan
415 (September, 2004), SSH data showed pre-existing cyclonic circulation in the areas

where the extreme cooling occurred. North of the warm core eddy, maximum cooling occurred 40 to 90 km east of Ivan's track in the area of maximum SSH change. Its location agreed well with the results of Price (1981), who found that maximum cooling for rapidly moving hurricanes usually occurs 30-150 km to the right of the track. However, another maximum cooling also occurred within the area of cyclonic circulation south of the warm core eddy, closest to Ivan's track. This large cooling effect extended further west than would have been expected based on previous research. Our results suggested that the observed extreme cooling was possibly due to strong upwelling caused by the bathymetric steering.

5. Summary

In this paper, we illustrate an application of a multiple domain modeling development study using a simulation of the ocean response to typhoon Kai-Tak. An intense nonlinear mesoscale eddy was generated with a Rossby radius of O (50-100km) horizontal scale in the northeastern SCS. Inertial oscillation was clearly observed. For the first few modeled days, advection dominated as the strong wind shear drove the mixed layer flows outward, away from the typhoon center, thus forcing upwelling from deep levels with correspondingly large upwelling velocities (>30-50 m/day). The surface mixed layer deepened as the thermocline rose and caused deeper convergence. The mixed layer and thermocline merged after July 6, when the thermocline water mixed to the surface rapidly due to wind-generated turbulence. A SST drop more than 9°C was found in both observation and simulation. This significant SST drop resulted from the influence of a slow moving typhoon, initial stratification and bathymetry-induced upwelling in the region where the typhoon hovered.

Acknowledgment

The authors acknowledge the computing resource of National Center for High Performance Computing, Taiwan. Comments from the two anonymous reviewers are deeply appreciated. Financial support for this work was provided by National Science Council, Taiwan (grant NSC972628M002001). Dr. S. Jan was granted by Taiwan's National Applied Research Laboratories under grant 97-TORI-007.

References:

Chang, S. W., and R. A. Anthes (1978), Numerical simulations of the ocean's nonlinear baroclinic response to translating hurricanes, *J. of Phys. Oceanogr.*, 8, 468-480.

Chen, Y. K. (2006), Typhoon-induced inertial motion in the South China Sea. Master thesis, Institute of Oceanography, National Taiwan University, 98 pp. (in Chinese)

Dietrich, D. E. (1997), Application of a modified ''a'' grid ocean model having reduced numerical dispersion to the Gulf of Mexico circulation, *Dyn. Atmos. Oceans*, 27, 201–217.

Dietrich, D. E., A. Mehra, R. L. Haney, M. J. Bowman, and Y.-H. Tseng (2004a), Dissipation effects in North Atlantic Ocean modeling, *Geophys. Res. Lett.*, 31, L05302, doi:10.1029/2003GL019015.

Dietrich, D. E., R. L. Haney, V. Fernandez, S. Josey and J. Tintore (2004b), Air-sea fluxes based on observed annual cycle surface climatology and ocean model internal dynamics: A precise, non-damping zero-phase-lag approach applied to the Mediterranean Sea, *J. Mar. Syst.*, 52, 145–165.

Dietrich, D. E., Y. H. Tseng, S. Jan, P. Yau, C. Lin and X. Wang (2007), Modeled ocean response to Hurricane Katrina (extended abstract), The 16th Conference on Atmospheric and Oceanic Fluid Dynamics, Santa Fe, New Mexico, 25-29, June.

Dietrich, D. E., Y. H. Tseng, R. Medina, S. A. Piacsek, M. Liste, M. Olabarrieta, M. J. Bowman, and A. Mehra (2008), Mediterranean Overflow Water (MOW) simulation using a coupled multiple-grid Mediterranean Sea/North Atlantic Ocean model, *J. Geophys. Res.*, 113, C07027, doi:10.1029/2006JC003914.

Emanuel, K. A. (1986), An air-sea interaction theory for tropical cyclones Part I, *J. Atmos. Sci.*, 42, 1062-1071.

471 Emanuel, K. A., (1999), Thermodynamic control of hurricane intensity, *Nature*, 401, 665-669.
472 Emanuel, K. (2001), Contribution of tropical cyclones to meridional heat transport by the
473 oceans, *J. Geophys. Res.*, 106, 14771-14781.
474 Gill, A. E. (1982), *Atmosphere-Ocean Dynamics*, 622 pp., Academic, New York.
475 Hellerman, S., and M. Rosenstein (1983), Normal monthly wind stress over the world ocean
476 with error estimates, *J. Phys. Oceanogr.*, 13, 1093-1104.
477 Jacob, S .D., L. K. Shay, and A. J. Mariano (2000), The 3D oceanic mixed layer response to
478 Hurricane Gilbert, *J. Phys. Oceanogr.*, 14, 59-78.
479 Jacob, S. D., and L. K. Shay (2003), The role of oceanic mesoscale features on the tropical
480 cyclone–induced mixed layer response: A case study, *J. Phys. Oceanogr.*, 33, 649-676.
481 Large, W. G., and S. Pond (1981), Open ocean flux measurements in moderate to strong winds,
482 *J. Phys. Oceanogr.*, 11, 324-336.
483 Levitus, S., and T. Boyer (1994), World Ocean Atlas 1994, vol. 4, Temperature, 150 pp.,
484 NOAA Atlas NESDIS 4.
485 Lin, I., W. T. Liu, C. Wu, G. T. F. Wong, C. Hu, Z. Chen, W. Liang, Y. Yang, and K. Liu
486 (2003), New evidence for enhanced ocean primary production triggered by tropical
487 cyclone, *Geophys. Res. Lett.*, 30, 1781, doi:10.1029/2003GL017141.
488 Lin, I.-I., C.-C. Wu, K. A. Emanuel, I.-H. Lee, C.-R. Wu and I.-F. Pun (2005), The interaction
489 of Supertyphoon Maemi (2003) with a warm ocean eddy, *Mon. Weather Rev.*, 133,
490 2635-2649.
491 Lin I.-I., I.-F.Pun, and Wu, C.-C. Wu (2009b), Upper ocean thermal structure and the western
492 north Pacific category-5 typhoons. Part II: Dependence on translation speed, in press,
493 *Mon. Weather Rev.*
494 Lin I.-I., C.-H. Chen, I.-F. Pun, W. T. Liu, and C.-C. Wu (2009a), Warm ocean anomaly, air
495 Sea fluxes, and the rapid intensification of tropical cyclone Nargis (2008), *Geophys. Res.*
496 *Lett.*, 36, L03817, doi:10.1029/2008GL035815.

497 Lin I.-I., C.-C. Wu, I.-F. Pun, and D.-S. Ko (2008), Upper-ocean thermal structure and the
498 western north Pacific category 5 typhoons. Part I: Ocean features and the category 5
499 typhoons' intensification, *Mon. Weather Rev.*, 136, 3288–3306.
500 Moon, I.-J., I. Ginis and T. Hara (2008), Impact of the reduced drag coefficient on ocean wave
501 modeling under hurricane conditions, *Mon. Weather Rev.*, 136, 1217-1223
502 Moon, I.-J., I. Ginis, T. Hara and B. Thomas (2007), A Physics-based parameterization of
503 air-sea momentum flux at high wind speeds and its impact on hurricane intensity
504 predictions, *Mon. Weather Rev.*, 135, 2869-2878.
505 Oey, L.-Y., T. Ezer, D.-P. Wang, X.-Q. Yin and S.-J. Fan (2006), Loop Current warming by
506 Hurricane Wilma., *Geophys. Res. Lett.*, 33, L08613.
507 Oey, L.-Y., T. Ezer, D.-P. Wang, X.-Q. Yin and S.-J. Fan (2007), Hurricane-induced motions
508 and interaction with ocean currents, *Cont. Shelf Res.*, 27, 1249-1263.
509 Pacanowski, R. C. and S. G. H. Philander (1981), Parameterization of vertical mixing in
510 numerical models of tropical oceans, *J. Phys. Oceanogr.*, 30, 1069-1082.
511 Prasad, T. G. and P. J. Hogan (2007), Upper-ocean response to Hurricane Ivan in a 1/25°
512 nested Gulf of Mexico HYCOM, *J. Geophys. Res.*, *112*, C04013,
513 doi:10.1029/2006JC003695.
514 Price, J. F. (1981), Upper ocean response to a hurricane, *J. Phys. Oceanogr.*, 11, 153-175.
515 Price, J. F., T. B. Sanford and G. Z. Forristall (1994), Forced stage response to a moving
516 hurricane, *J. Phys. Oceanogr.*, 24, 233-260.
517 Powell, M. D., P. J. Vichery, T. Reinhold (2003), Reduced drag coefficient for high wind
518 speeds in tropical cyclones, *Nature*, 422, 279-283.
519 Qu, T., Y. Du, J. Gan, and D. Wang (2007), Mean seasonal cycle of isothermal depth in the
520 South China Sea, *J. Geophys. Res.*, *112*, C02020, doi:10.1029/2006JC003583.
521 Shay, L. K., R. L. Elsberry, and P. G. Black (1989), Vertical structure of the ocean current
522 response to a hurricane, *J. Phys. Oceanogr.*, 19, 649-669.

523 Shay, L. K., G. J. Goni, and P. G. Black (2000), Effects of a warm oceanic feature on
524 Hurricane Opal, *Mon. Weather Rev.*, 128, 1366-1383.
525 Shang, S.-L., L. Li, F. Sun, J. Wu, C. Hu, D. Chen, X. Ning, Y. Qiu, C. Zhang, S. Shang
526 (2008), Changes of temperature and bio-optical properties in the South China Sea in
527 response to typhoon Lingling, 2001., *Geophys. Res. Lett.*, 35, L10602.
528 doi:10.1029/2008GL033502.
529 Sheng, J., X. Zhai, R. J. Greatbatch (2006), Numerical study of the storm-induced circulation
530 on the Scotian Shelf during Hurricane Juan using a nested-grid ocean model, *Prog.*
531 *Oceanogr.*, 70, 233-254..
532 Sheng, J., L. Wang, S. Androfouot, C. Hu, B. G. Hatcher, F. E. Muller-Karger, B. Kjerfve, W.
533 D. Heyman, and B. Yang (2007), Upper ocean response of the Mesoamerican Barrier
534 Reef System to Hurricane Mitch and coastal freshwater inputs: A study using
535 Sea-viewing Wide Field-of-view Sensor (SeaWiFS) ocean color data and a nested-grid
536 ocean circulation model, *J. Geophys. Res.*, 112*, C07016, doi:10.1029/2006JC003900.*
537 Tsai, Y., C.-S. Chern, J. Wang (2008), The upper ocean response to a moving typhoon, *J.*
538 *Oceanogr.*, 64, 115-130.
539 Tseng, Y.-H., J. H. Ferziger and D. E. Dietrich (2005), Regional circulation of the Monterey
540 Bay region-hydrostatic versus non-hydrostatic modeling, *J. Geophys. Res.*, 110, C09015,
541 doi:10.1029/2003JC002153.
542 Tseng, Y. H. and D. E. Dietrich (2006), Entrainment and transport in the three-dimensional
543 idealized gravity current simulation, *J. Atmos. Ocean Tech.*, 23, 1249-1269.
544 Tseng, Y.-H., and L. C. Breaker (2007), Nonhydrostatic simulations of the regional circulation
545 in the Monterey Bay area, *J. Geophys. Res.*, 112, C12017, doi:10.1029/2007JC004093.
546 Tseng, Y.H. (2008), High-order Essentially Local Extremum Diminishing schemes for
547 environmental flows, *Int. J. Numer. Methods Fluids*, 58, 213-235.

548 Wu, C.-C., C.-Y Lee and I.-I. Lin (2007), The effect of the ocean eddy on tropical cyclone
549 intensity, *J. Atmos. Sci.*, 64, 3562-578.

550 Wu, C.-R., Y. L. Chang, L.-Y. Oey, J. Chang, C.W.-J. Chang, and Y.-C. Hsin (2008), Air-sea
551 interaction between tropical cyclone Nari and Kuroshio, *Geophys. Res. Lett.*, 35,
552 L12605, doi:10.1029/2008GL033942.

553 Zedler, S. E., T. D. Dickey, J. F. Doney, J. F. Price, X. Yu, and G. L. Mellor (2002), Analyses
554 and simulations of the upper ocean's response to Hurricane Felix at the Bermuda Testbed
555 Mooring site: 13-23 August 1995, *J. Geophy. Res.*, 107, C12, 3232,
556 doi:10.1029/2001JC000969.

Figure 1: Ten-days averaged SSH TOPEX/Poseidon images before and after typhoon Kai-Tak (June 26-July5 (a) and July 9-July 18 (b), respectively) from the satellite showing the passage of typhoon Kai-Tak in northeast South China Sea. Luzon Strait is between Taiwan and Philippine. The storm-track of typhoon Kai-Tak is superimposed.

Figure 2: Daily averaged QuikSCAT wind fields at 10 m from 7/3, 2000 (top left) to 7/7, 2000 (bottom center). The initial stratification (temperature and salinity) is shown in the bottom right panel, taken from the nearby SEAT station before the passage of Typhoon Kai-Tak. Observational stations: KA1 (o); SEAT (◇); and ST (□).

Figure 3: The dual-grid Pacific Ocean Model, DUPOM, uses two grids in order to resolve critical features in Asia Marginal Sea, such as the Luzon Strait.

Figure 4: Simulated surface current velocity and sea surface height (SSH) at different time.

Figure 5: Comparison of velocity profiles in the upper layer between the DUPOM and observation. Model (top), filtered observation (middle), observed raw data (bottom).

Figure 6: Time-series velocity components in the upper layer at different locations. Relative locations with respect to typhoon center: west, east, north, south (from top to bottom).

Figure 7: (a) Comparison of time-series surface temperature between different turbulent parameterization schemes at the south tip of Taiwan. (b) Comparison of time-series surface temperature between different wind stress intensity at the south tip of Taiwan.

Figure 8: (a) Horizontal SST distribution along latitude, (top) and longitude (bottom). (b) Modeled SST distribution at hour 90.

Figure 9: Time-series temperature in the upper layer at different locations along latitude 20.5°N. (a) 116.5°E; (b) 118.5°E; (c) 119°E; and (d) 120.375°E.

Figure 10: Daily averaged vertical velocity at 45 m depth for day 5 (7/7).

Figure 11: Daily averaged bottom current vectors just above the bottom cell for day 4 (a) and day 5 (b). The bathymetry is colored as contours.

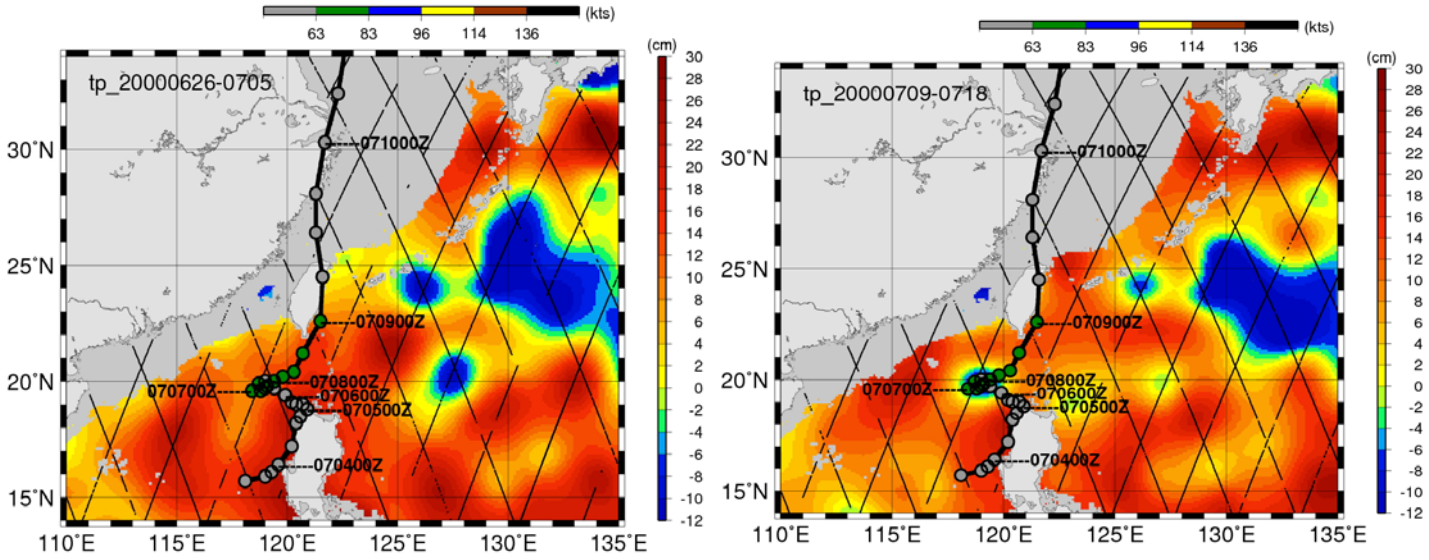
(kts)
63
83
96
114
136
(cm)
30
28
26
24
22
20
18
16
14
12
10
8
6
4
2
0
-2
-4
-6
-8
-10
-12
tp_20000626-0705
0710000Z
0709000Z
0708000Z
0707000Z
0706000Z
0705000Z
0704000Z
30°N
25°N
20°N
15°N
110°E
115°E
120°E
125°E
130°E
135°E
tp_20000709-0718
0710000Z
0709000Z
0708000Z
0707000Z
0706000Z
0705000Z
0704000Z

(a) (b)

Figure 1

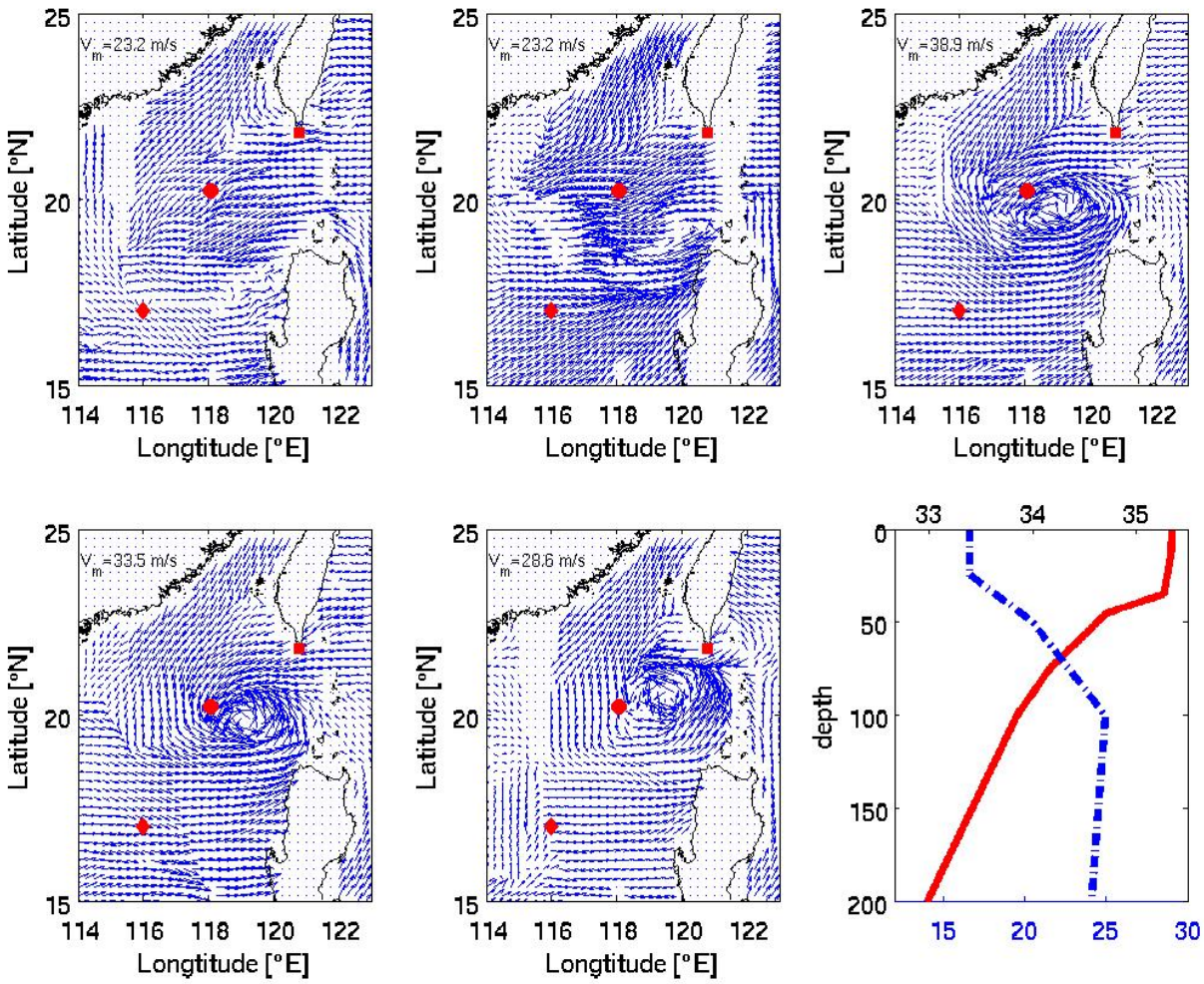
V_m =23.2 m/s
V_m =23.2 m/s
V_m =38.9 m/s
V_m =33.5 m/s
V_m =28.6 m/s
Latitude [°N]
Longtitude [°E]
depth
25
20
15
114
116
118
120
122
33
34
35
0
50
100
150
200
15
20
25
30

Figure 2

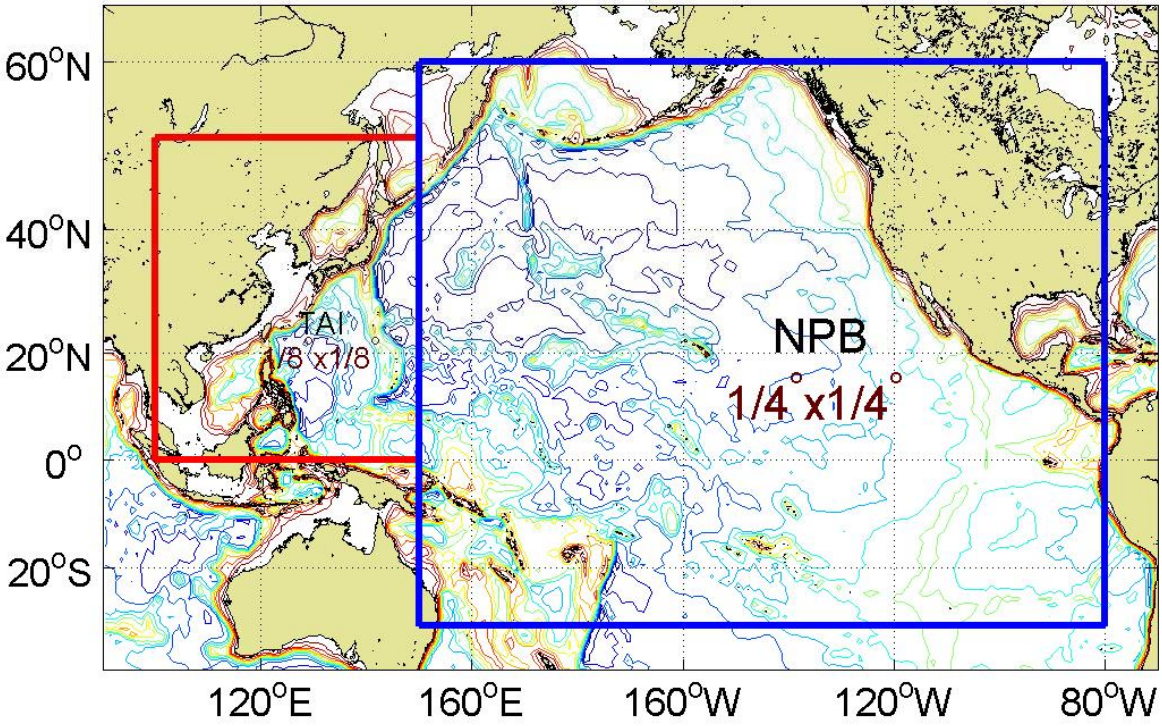

Figure 3

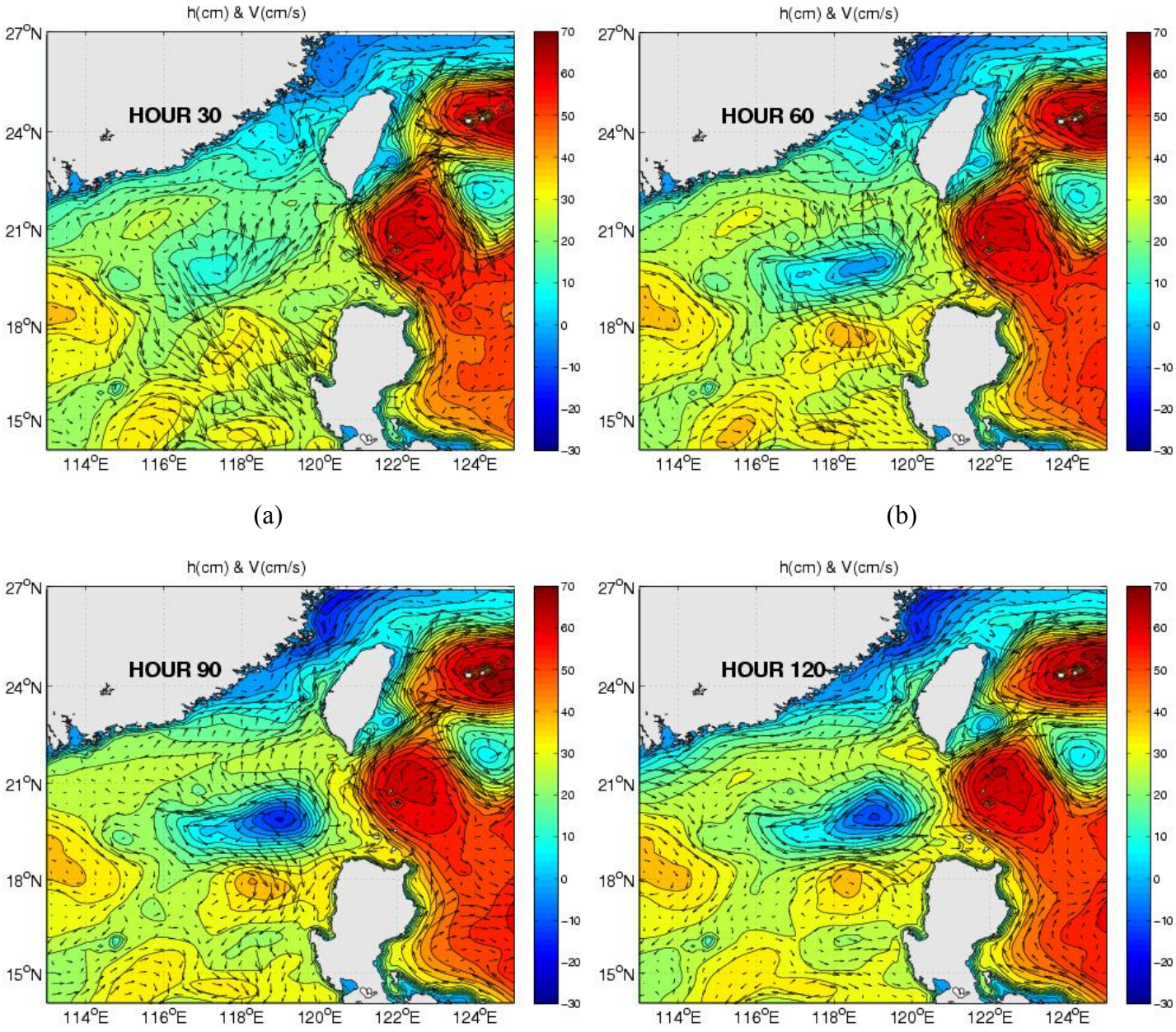

(a) (b)

(c) (d)

Figure 4

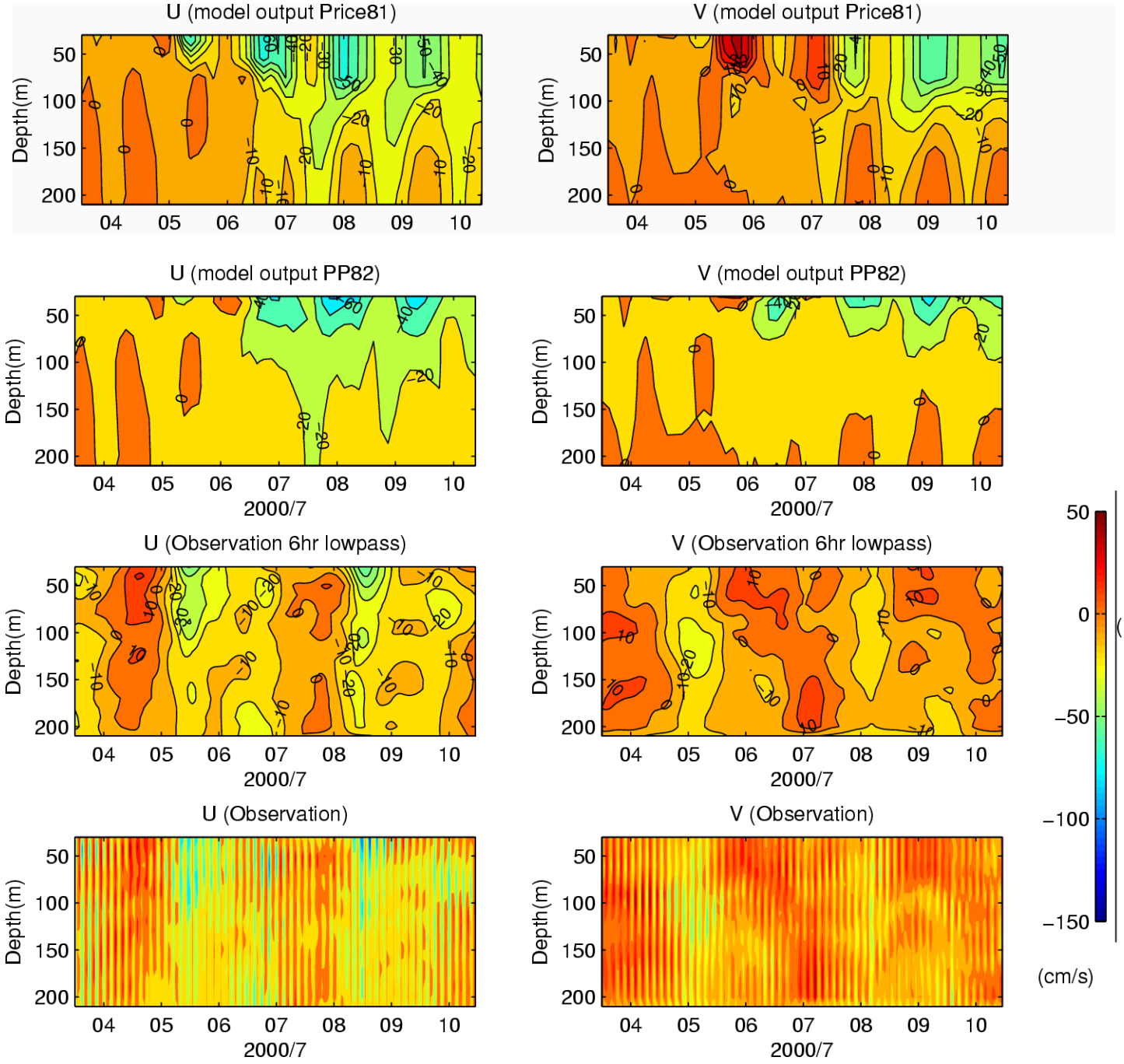
U (model output Price81)
V (model output Price81)
U (model output PP82)
V (model output PP82)
U (Observation 6hr lowpass)
V (Observation 6hr lowpass)
U (Observation)
V (Observation)
Depth(m)
2000/7
(cm/s)

Figure 5

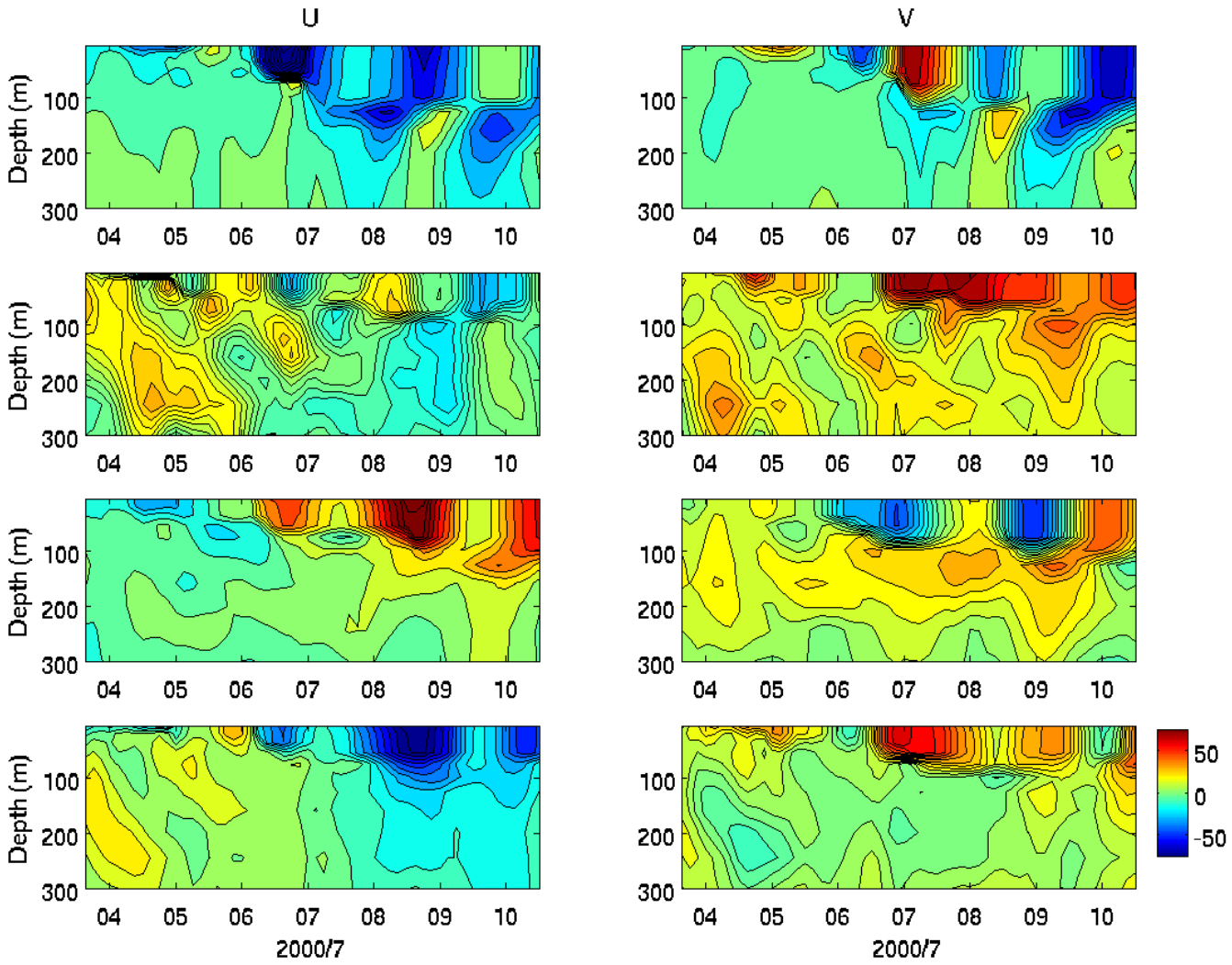

Figure 6

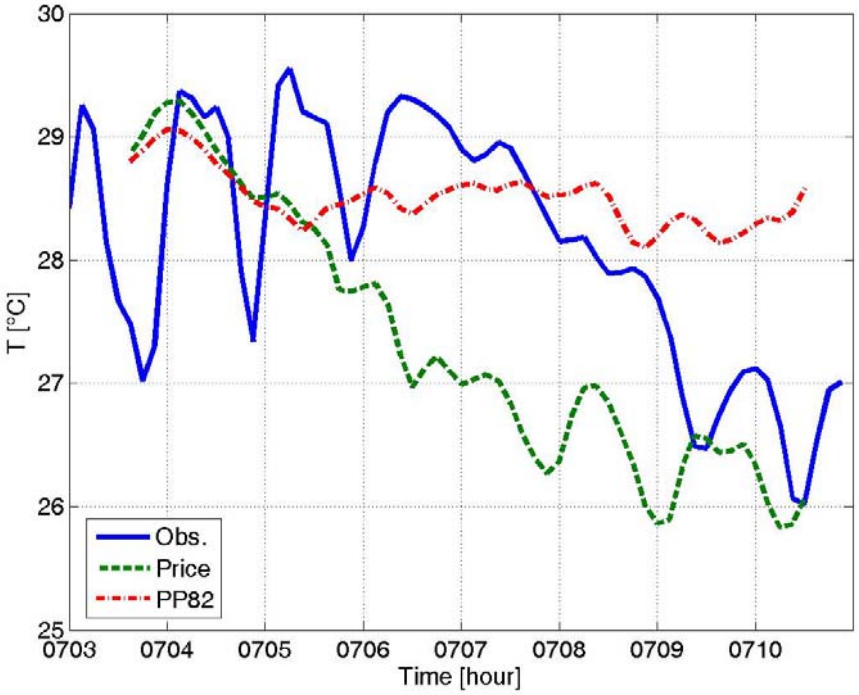
30
29
28
27
26
25
T [°C]
0703
0704
0705
0706
0707
0708
0709
0710
Time [hour]
Obs.
Price
PP82

(a)

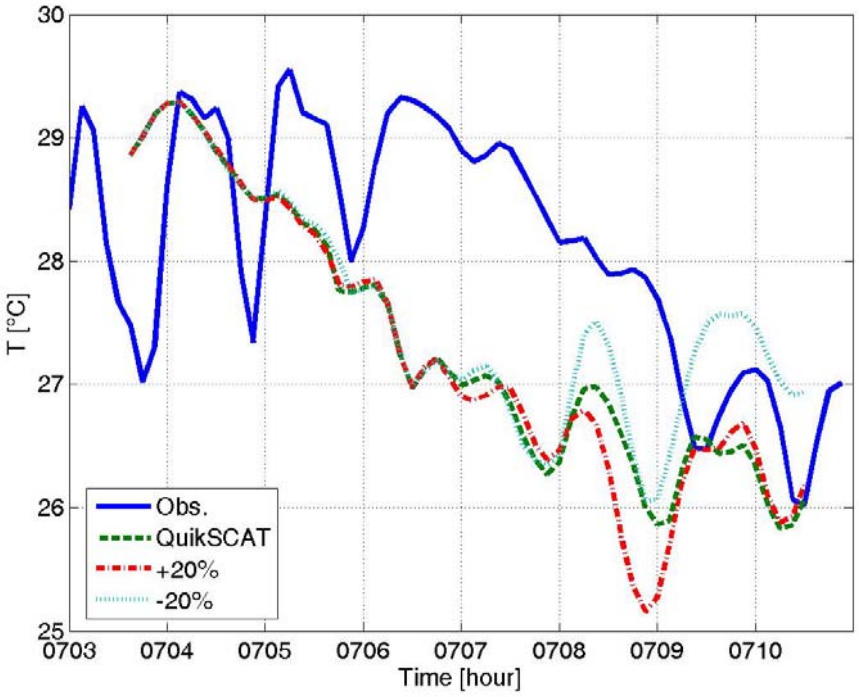
30
29
28
27
26
25
T [°C]
0703
0704
0705
0706
0707
0708
0709
0710
Time [hour]
Obs.
QuikSCAT
+20%
-20%

(b)

Figure 7

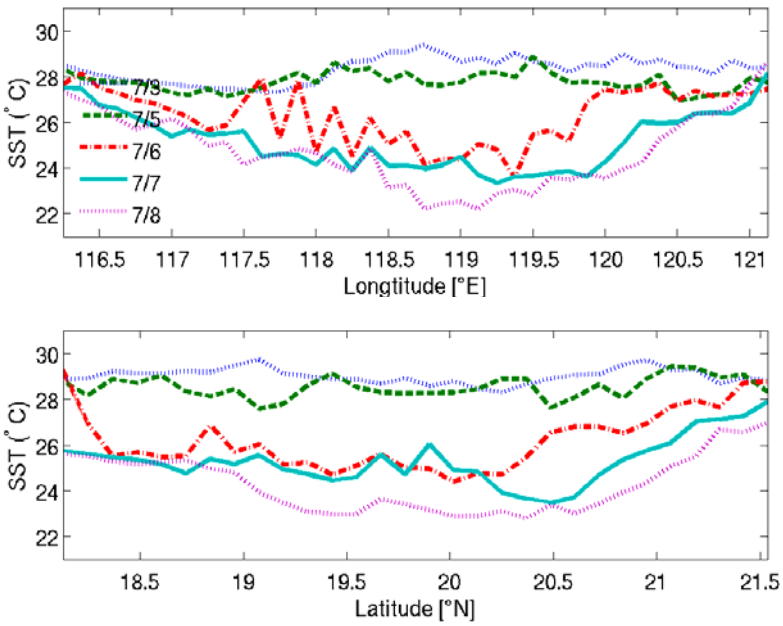
SST (°C)
7/3
7/5
7/6
7/7
7/8
Longtitude [°E]
Latitude [°N]

(a)

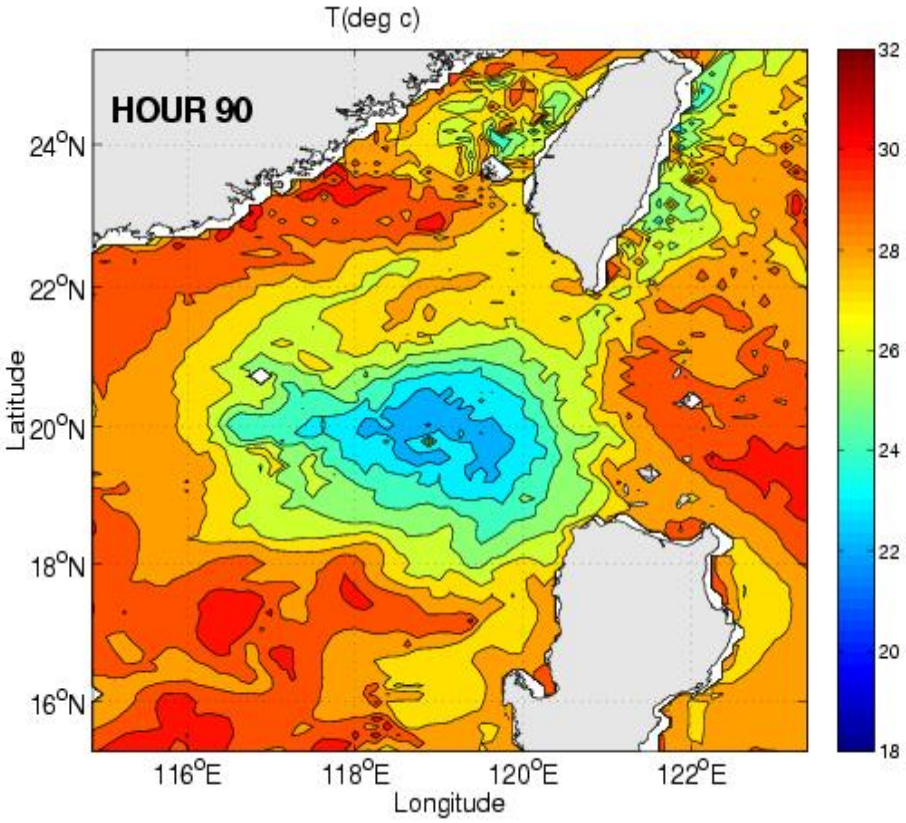
T(deg c)
HOUR 90
24°N
22°N
20°N
18°N
16°N
Latitude
116°E
118°E
120°E
122°E
Longitude

(b)

Figure 8

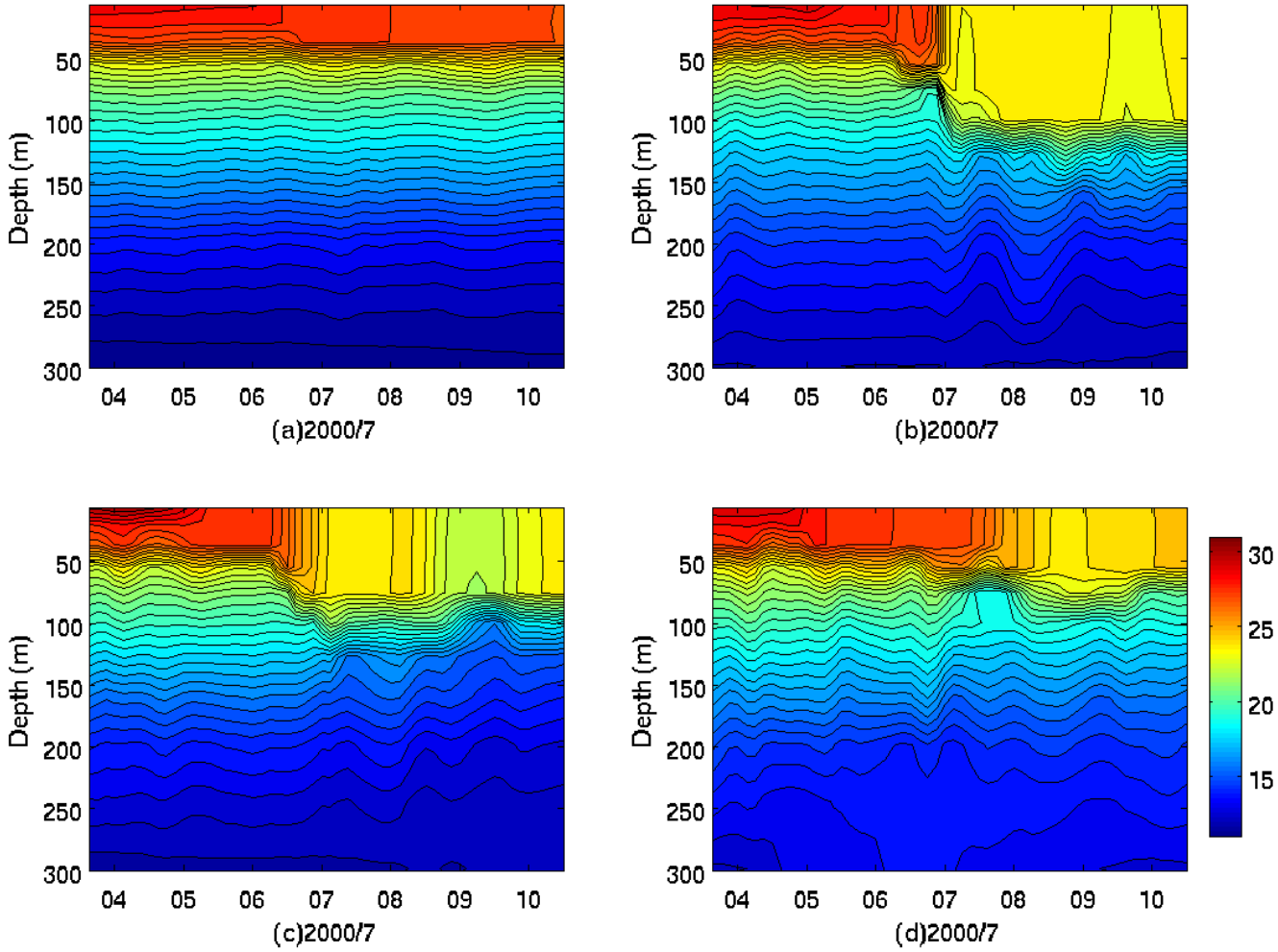
Depth (m)
50
100
150
200
250
300
04
05
06
07
08
09
10
(a)2000/7
(b)2000/7
(c)2000/7
(d)2000/7
30
25
20
15

Figure 9

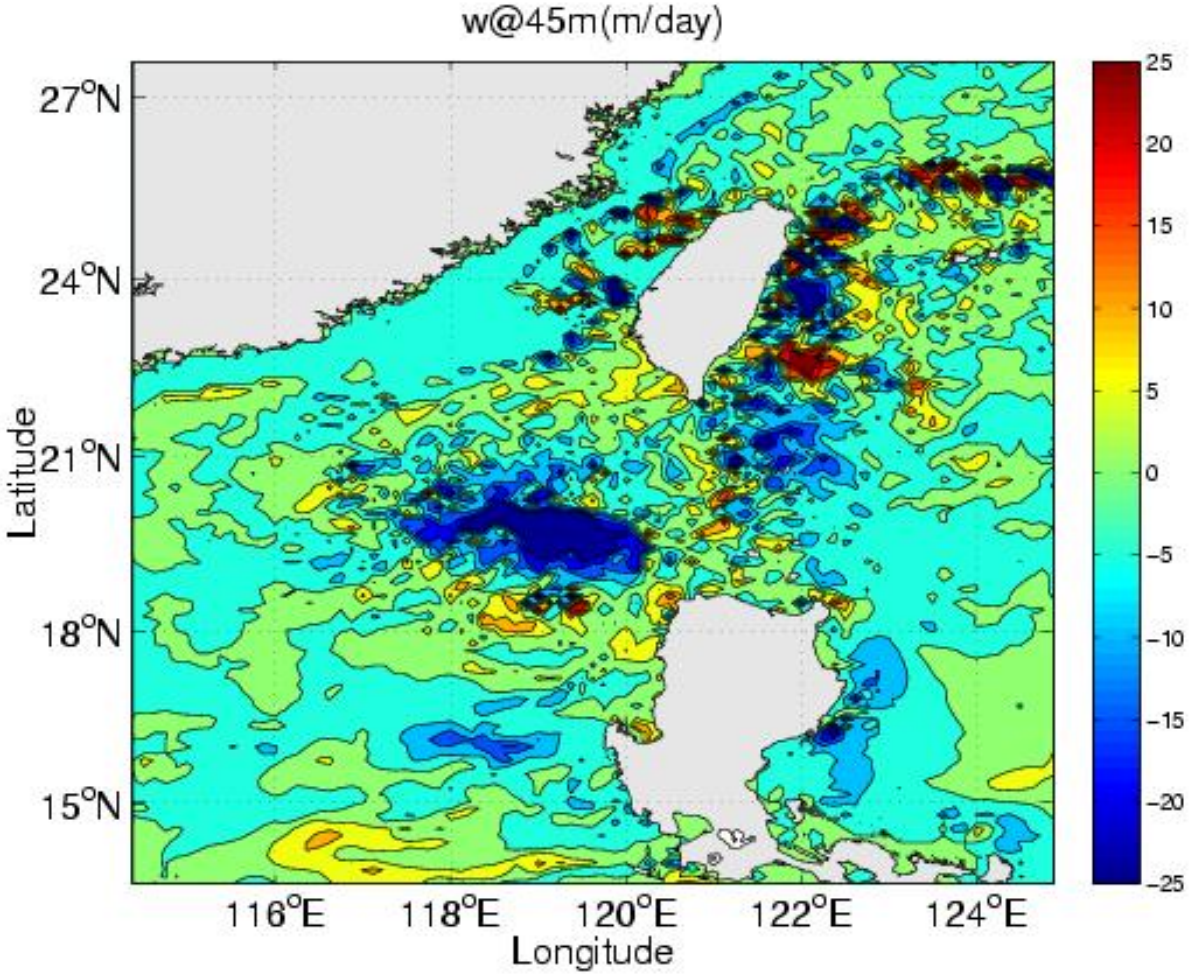
w@45m(m/day)
27°N
24°N
21°N
18°N
15°N
Latitude
116°E
118°E
120°E
122°E
124°E
Longitude
25
20
15
10
5
0
−5
−10
−15
−20
−25

Figure 10

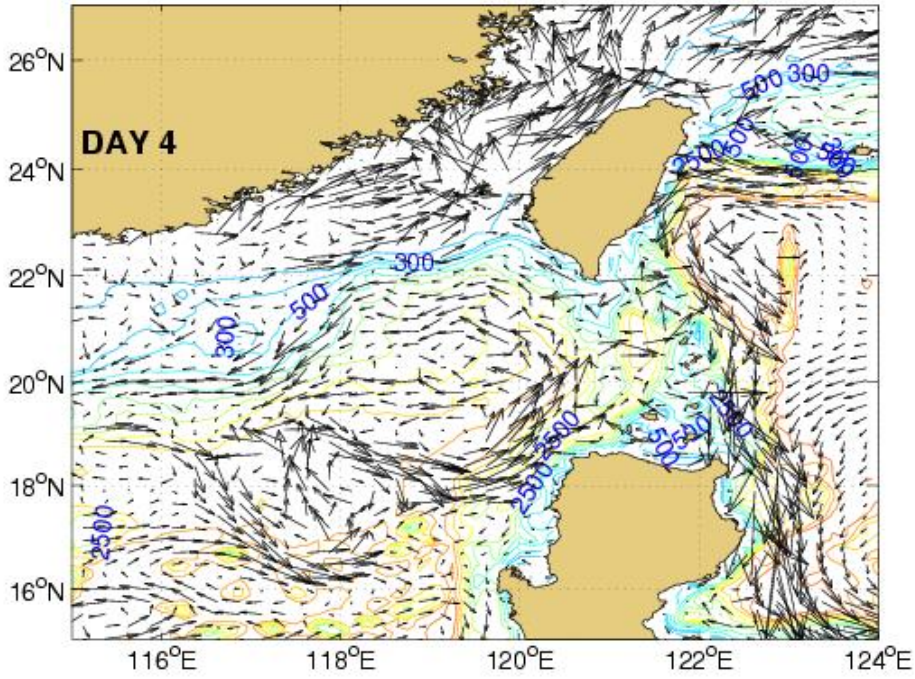
DAY 4
26°N
24°N
22°N
20°N
18°N
16°N
116°E
118°E
120°E
122°E
124°E
300
500
2500

(a)

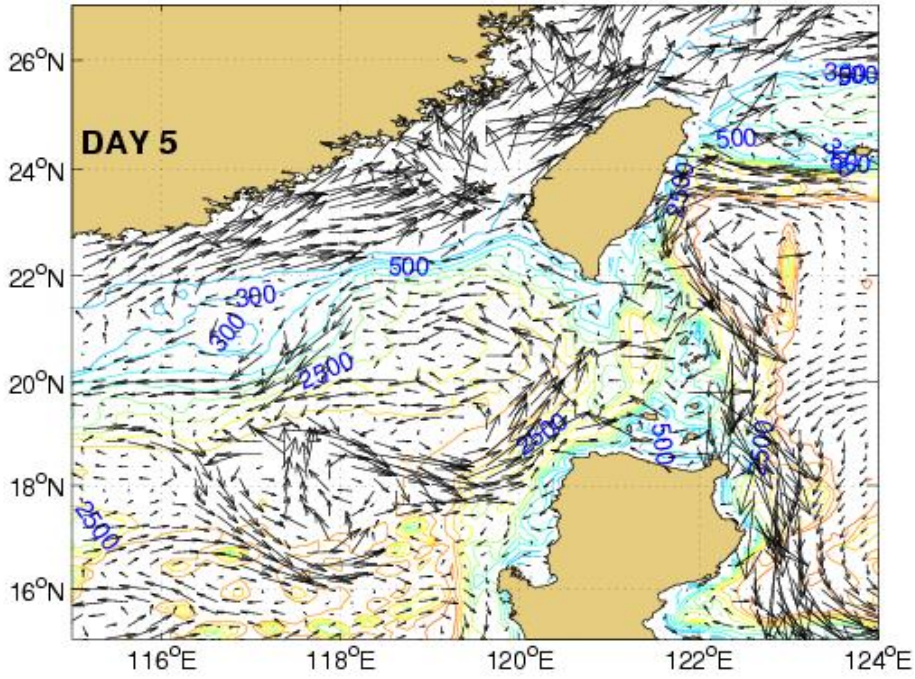
DAY 5
26°N
24°N
22°N
20°N
18°N
16°N
116°E
118°E
120°E
122°E
124°E
300
500
2500

(b)

Figure 11